Low-field quantum Hall transport in an electron Fabry-Perot interferometer: Dependence of constriction filling on front-gate voltage

Ping V. Lin, F. E. Camino,* and V. J. Goldman
Department of Physics, Stony Brook University, Stony Brook, New York 11794-3800, USA
(Received 20 August 2008; revised manuscript received 5 November 2008; published 29 December 2008)

We report systematic quantum Hall transport experiments on Fabry-Perot electron interferometers at ultralow temperatures. The GaAs/AlGaAs heterostructure devices consist of two constrictions defined by etch trenches in the two-dimensional electron layer, enclosing an approximately circular island. Front gates deposited in etch trenches allow one to change the constriction filling, relative to the bulk. A systematic variation of the front-gate voltage affects the constriction and the island electron density, while the bulk density remains unaffected. This results in quantized plateaus in longitudinal resistance, while the Hall resistance is dominated by the low-density, low-filling constriction. At lower fields, when the quantum Hall plateaus fail to develop, we observe bulk Shubnikov-de Haas oscillations in series corresponding to an integer filling of the magnetoelectric subbands in the constrictions. This shows that the whole interferometer region is still quantum coherent at these lower fields at 10 mK. Analyzing the data within a Fock-Darwin model, we obtain the constriction electron density as a function of the front-gate bias and, extrapolating to the zero field, the number of electric subbands (conductance channels) resulting from the electron confinement in the constrictions.

DOI: 10.1103/PhysRevB.78.245322 PACS number(s): 73.43.Fj

I. INTRODUCTION

There has been a continuing wealth of research into the ground-state and transport properties of confined two-dimensional (2D) electron systems ever since the discovery of the integer quantum Hall effect[1] (IQHE) and development of lithographic techniques. The IQHE can be understood in terms of transport by one-dimensional (1D) chiral edge channels corresponding to an integer number of fully occupied Landau levels.[2–4] In this picture, near an integral Landau level filling $\nu \approx f$, when the chemical potential lies in the gap of localized bulk states, the current is carried by dissipationless edge channels and the Hall resistance is quantized exactly to h/fe^2. Dissipative transport occurs when current is carried by the extended bulk states of the partially occupied topmost Landau level, between the plateaus. Such interpretation of the IQHE of noninteracting electrons in terms of edge channels is straightforward since for noninteracting electrons the edge channels are formed in one-to-one correspondence with the bulk Landau levels. Including effects of electron interaction is not so straightforward, but, qualitatively, the concept of current-carrying chiral edge channels is still applicable.[5–10]

In a constricted geometry, even in zero magnetic field $B=0$, an approximate quantization of conductance[11,12] is understood as resulting from size-quantized nonchiral 1D conducting channels passing through the constriction.[13] In a quantizing B, the size-quantized and the chiral edge channels hybridize, there exists a transitional regime where both effects co-exist, and the plateau positions in B depend on both size and Landau quantization. Here, the noninteracting electron theory does not provide a quantitatively accurate description so that effects of interaction resulting in a self-consistent confining potential have to be included. In addition, in such constrictions, "backscattering" by quantum tunneling between the extended edge states is possible and leads to a deviation from exact plateau quantization.

In this paper we present a comprehensive experimental characterization of quantum Hall (QH) and Shubnikov-de Haas (SdH) transport in an electron Fabry-Perot interferometer.[14–16] The constrictions are wide: we obtain the zero-B number of conduction channels between 10 and ~500. Similar electron interferometer devices have been studied by others in the integer QH regime.[17–19] Earlier studies of dependence of constriction electron density were done in single unetched quantum point contacts defined by the split-gate technique, where the number of conductance channels was varied between zero (pinch-off) and a dozen.[11–13] Indeed, one reason why no similar work was feasible earlier is that in our devices, the main depletion is provided by etching so that the constriction density can be varied in a wide range while maintaining the device geometry. In the front-gate-only device of Ref. 17, changing gate voltage appreciably either opens or closes the constrictions completely so that the intended device geometry is lost.

Our experiments on the interferometers in the low-field integer QH regime reported here are moreover motivated by application of such devices in the fractional QH regime, where interference of fractionally charged Laughlin quasiparticles has been reported.[20–25] Additional motivation is provided by proposed application of such Fabry-Perot interferometers, in conjunction with quantum antidots,[26] to detection of non-Abelian braiding statistics and as a physical implementation of topological quantum computation.[27–30]

II. SAMPLES AND EXPERIMENTAL TECHNIQUES

The interferometer sample was fabricated from a very low disorder double-δ-doped GaAs/AlGaAs heterostructure.[31] The 2D electron system is buried 320 nm below the surface. First, ohmic contacts are formed on a pre-etched mesa. Then etch trenches are defined by electron-beam lithography, using proximity correction software for better definition of narrow and long gaps between the exposed areas. After a shallow

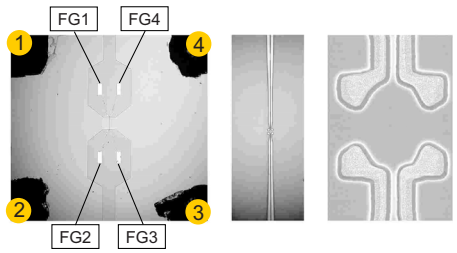

FIG. 1. (Color online) A Fabry-Perot electron interferometer device. Optical (two left) and scanning electron (SEM, right) micrographs of the interferometer sample. Numbered circles on the four corners of the 4×4 mm^2 mesa show ohmic contacts to 2D bulk electron layer. Four front gates (FG1–4) are deposited in shallow etch trenches, defining a circular island separated from the 2D bulk by two 1.2-μm wide constrictions. In a quantizing magnetic field, chiral edge channels follow an equipotential at the periphery of the undepleted 2D electrons. Longitudinal R_{XX} (current 1–4, voltage 2–3) and Hall R_{XY} (current 2–4, voltage 1–3) resistances are measured. The back gate (not shown) extends over the entire sample.

160 nm wet etch, 50 nm thick Au/Ti front-gate (FG) metallization is deposited in a self-aligned process. Finally, samples are mounted on sapphire substrates with In metal, which serves as the global back gate. The interferometer sample studied in this paper is the same as in Ref. 24, but on a subsequent cooldown and under different illumination.

Samples were cooled in the tail of the mixing chamber of a top-loading into mixture dilution ^{3}He-^{4}He refrigerator. A bulk 2D electron density $n_B=1.16\times10^{11}$ cm^{-2} was achieved after illumination by a red light emitting diode (LED) at 4.2 K. All experiments reported in this work were performed at the fixed bath temperature of 10 mK, calibrated by nuclear orientation thermometry. Extensive cold filtering in the electrical leads attenuates the electromagnetic background "noise" incident on a sample, allowing one to achieve effective electron temperatures of $\leq$15 mK.[23] Four-terminal longitudinal $R_{XX}=V_X/I_X$ and Hall $R_{XY}=V_Y/I_X$ magnetoresistances, see Fig. 1, were measured with a lock-in technique at 5.4 Hz. The excitation current was set so as to keep the larger Hall or longitudinal voltage ≤5 μV.

III. EXPERIMENTAL RESULTS AND ANALYSIS

A. Magnetotransport

Figures 2–4 summarize experimental longitudinal and Hall four-terminal magnetoresistance in sample M97Ce, the same as reported in Ref. 24, but under different illumination, taken in a range of front-gate voltages $-580\text{ mV}\leq V_{\rm FG}\leq+100$ mV. Even at zero front gate $V_{\rm FG}=0$, the GaAs surface depletion of the etch trenches, which remove the doping layer, creates an electron confining potential so that the constriction and the island electron densities are less than the 2D "bulk." Application of a negative $V_{\rm FG}$ depletes the constriction and the island region of the sample further. The two constrictions were tuned for approximate symmetry by application of a constant ±20 mV differential bias between FG1 and FG4, additional to the common front-gate bias given in this paper as $V_{\rm FG}$. Detuning front-gate voltage from symmetry allows one to verify each constriction filling separately.

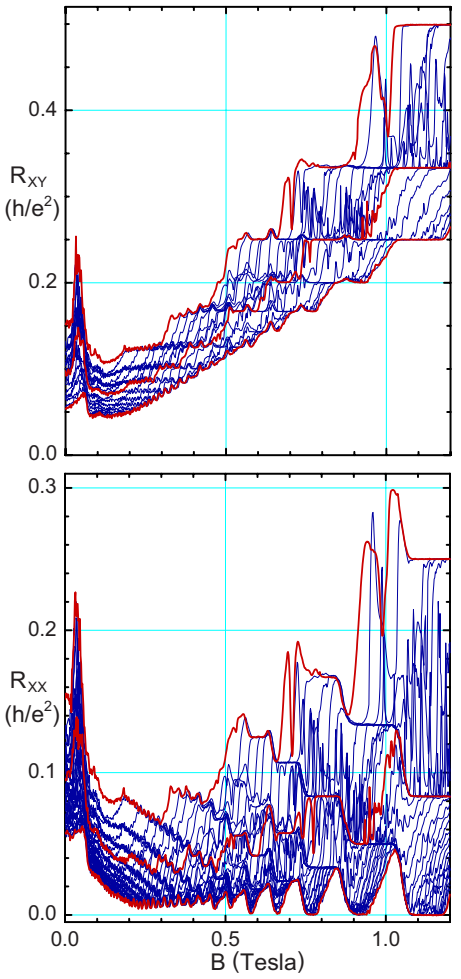

FIG. 2. (Color online) Representative longitudinal and Hall magnetoresistance traces of the interferometer sample. The front-gate voltage is stepped by multiples of 20 mV in the range $-580\text{ mV}\leq V_{\rm FG}\leq+100$ mV. The zero resistance level is the same for all traces. Application of $V_{\rm FG}$ changes the electron density in the interferometer region, both the island and the constrictions, thus shifting the B positions of the quantized plateaus. The smallest filling factor, that in constrictions, determines R_{XY}, while R_{XX} depends on filling in all regions of the sample: constrictions and the 2D bulk. Thick red traces: the lowest is at +100 mV, the middle at −360 mV, and the top (lowest electron density) at −580 mV.

Because in a uniform applied B the Landau-level filling factor $\nu=hn/eB$ is proportional to the local electron density n, in the depleted regions of the sample, ν is different from the 2D bulk ν_B. While $\nu\propto n/B$ is a variable, the quantum Hall exact filling f is a quantum number defined by the quantized Hall resistance as $f=h/e^2R_{XY}$. Because QH plateaus have finite width, regions with different ν may have the same f. In samples with lithographic constrictions, in general, there are two possibilities: (i) when depletion is small and on a wide QH plateau, the whole sample may have the same QH filling f; and (ii) more often, the constriction filling f_C and the bulk filling f_B are different. As can be seen in Fig. 2, as the front gates are biased more negative, there is a continuous series of well-developed constriction QH plateaus for

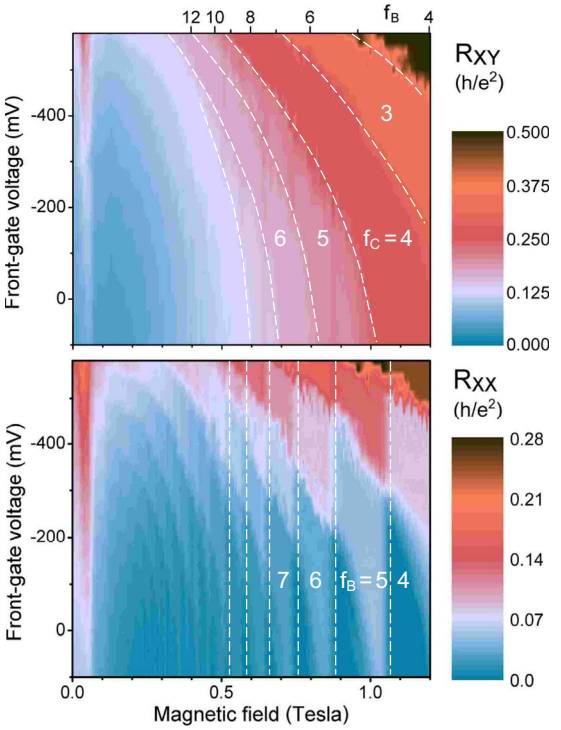

FIG. 3. (Color online) Color-mapped plot of the magnetoresistance data of Fig. 2. The Hall R_{XY} and longitudinal R_{XX} plateau regions are seen as the same shade. Note that the constriction filling factors are shifted to lower magnetic fields by a negative front-gate voltage, while the bulk is not affected. The absolute resistance values of the R_{XX} plateaus allows one to determine both constriction and bulk fillings as functions of magnetic field, as shown. The dashed white lines give approximate boundaries between consecutive quantum Hall plateaus.

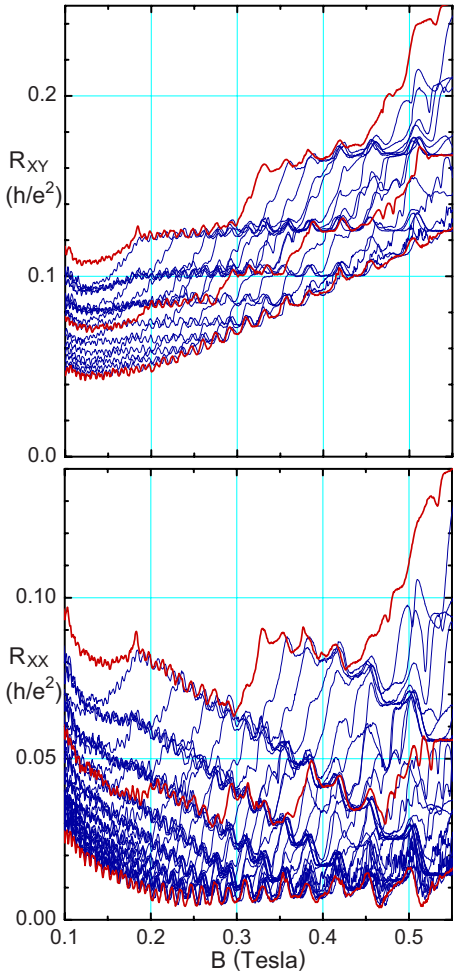

FIG. 4. (Color online) Blow up of the magnetoresistance data of Fig. 2 in the region of Shubnikov-de Haas oscillations and the developing quantum Hall plateaus in the bulk. Some traces are shown in thick red lines to help distinguish individual traces: the lowest is at +100 mV, the middle at −360 mV, and the top (lowest electron density) at −580 mV. Note that the B positions of the bulk SdH oscillations are not affected by V_{FG}, while superimposed on resistance background determined by the number of the conduction channels in the constrictions, which is shifted by V_{FG}. This allows us to separate the bulk and constriction features. The zero resistance level is the same for all traces.

each f_C, shifting to lower magnetic fields, and thus to higher f_B plateaus.

The Hall resistance R_{XY} allows us to determine the filling in the constrictions, the plateau positions in B giving definitive values of f_C. The longitudinal R_{XX} shows quantum Hall minima and quantized plateaus at $R_{XX}=(h/e^2)(1/f_C-1/f_B)$, when plateaus in constrictions and the bulk overlap in B.[32] Note the special case: when $f_C=f_B$, $R_{XX}=0$. Thus, a quantized plateau in $R_{XX}(B)$ implies quantum Hall plateaus for both the constriction region and the bulk, and a set of quantized $R_{XX}(B)$ plateaus provides definitive values for both f_C and f_B. Evolution of several stronger QH constriction and bulk plateaus as a function of V_{FG} are indicated in Fig. 3. As expected, the constriction plateaus are shifted to lower magnetic fields by a negative front-gate voltage, while the bulk plateaus are not affected.

Figure 4 shows detail of the magnetotransport data in the range of B where SdH oscillations in the bulk occur, transitioning to developing QH plateaus. As seen in the raw data, SdH oscillations are not shifted in B by front-gate bias; this is confirmed by Fourier analysis, which gives a V_{FG}-independent SdH oscillation frequency corresponding to the bulk density. The vertical positions of the bulk SdH oscillations are grouped in series corresponding to the number of conduction channels passing through the constriction. This shows as a constant resistance plateau in the Hall data, and a $(h/e^2)(1/f_C-1/f_B)$ background, the bulk Hall effect when f_C is constant, in the R_{XX} data. The values of the Hall plateaus and the $B=0$ intercept of the negative slope R_{XX} background are both h/f_Ce^2, which can be used to ascertain the channel number of the series.

It is not surprising that the QH edge channels pass through both constrictions. As can be seen in Fig. 4, there is a smooth, continuous transition from well-developed QH constriction plateaus to the low-field magnetoelectric conduction channel regime for each f_C series formed by various V_{FG} traces. This means that the whole interferometer region, including both constrictions, is quantum coherent even at 0.1 T, and most likely, indeed, even at $B=0$. If the two constrictions were not quantum coherent, their individual resistances

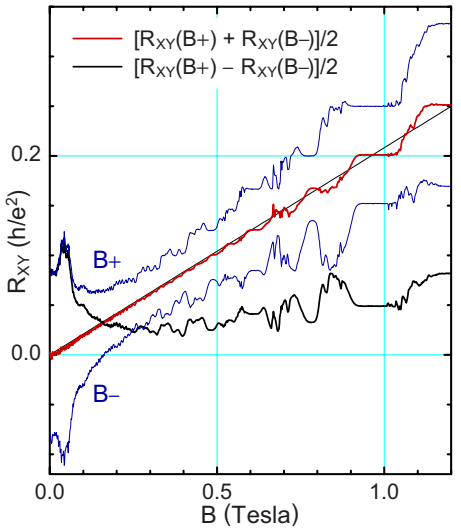

FIG. 5. (Color online) Experimental four-terminal Hall R_{XY} also contains longitudinal contribution. The two directly measured traces shown (thin blue lines) are obtained with magnetic field up ($B+$) and down ($B-$). The $R_{XY}(B-)$ trace is shown multiplied by -1, both horizontal and vertical axes. The middle trace (thick red line) is the average $\frac{1}{2}[R_{XY}(B+)+R_{XY}(B-)]$, which, according to Onsager relations, gives the true bulk R_{XY} (straight thin line gives the bulk density). Likewise, the difference $\frac{1}{2}[R_{XY}(B+)-R_{XY}(B-)]$ gives the longitudinal R_{XX}, which displays the quantized plateaus, e.g., $R_{XX}=0.05h/e^2$ ($f_C=4$ and $f_B=5$) at $B\approx 0.98$ T. Data taken at $V_{\mathrm{FG}}=-260$ mV.

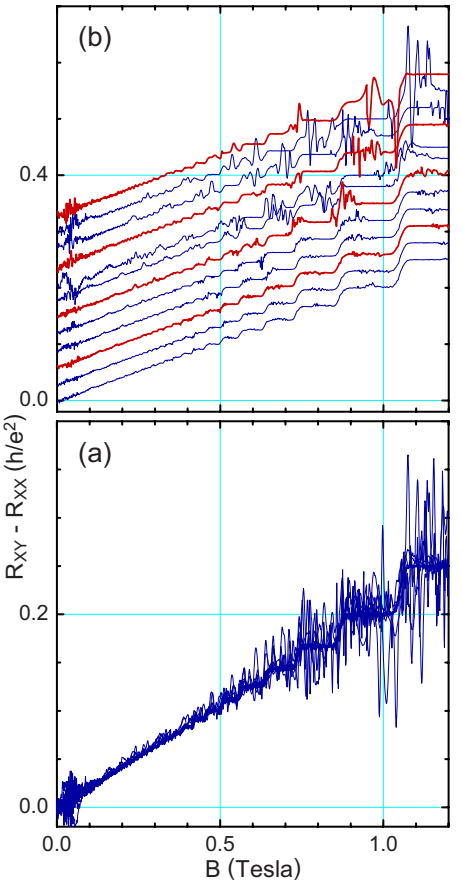

FIG. 6. (Color online) Representative traces illustrating subtraction of experimental Hall and longitudinal magnetoresistances at the same front-gate voltage. The lower panel shows the difference traces at various V_{FG}, all having true zero level. The subtraction results in the bulk Hall resistance (darker central region), with superimposed features due to mesoscopic effects and tunneling in the constrictions, different in each individual V_{FG} trace. The upper panel shows several individual V_{FG} traces shifted vertically by $0.01h/e^2$ per -20 mV of V_{FG}.

would add, which would be seen as an apparent doubling of the constriction channel number as B is lowered.

Because a four-terminal R_{XY} generally contains longitudinal contributions, it may not be clear-cut as to what is the true Hall effect. We can ascertain the assignment of various features to the bulk or to the constriction by the following two techniques. First, we can reverse the direction of the magnetic field, that is, take the corresponding magnetoresistance data at both $B+$, up, and $B-$, down (shown in Fig. 5). The $R_{XY}(B-)$ data are multiplied by -1, both the magnetic field and resistance. According to Onsager relations for a magnetoconductivity tensor in an inversion-symmetric sample,[33] the Hall contribution changes sign, while the diagonal contributions remain unaffected. Thus, the average Hall $\frac{1}{2}[R_{XY}(B+)+R_{XY}(B-)]$ corresponds to the true bulk Hall effect, with all longitudinal contributions to resistance, including the effect of constrictions, removed (within the experimental accuracy). The thin solid line in Fig. 5 gives the classical Hall slope corresponding to the bulk density $n_B=1.16\times 10^{11}$ cm^{-2}, obtained from the B positions of the V_{FG}-independent QH plateaus in Figs. 2 and 3; as can be seen, it matches the $B+$, $B-$ average slope well. The difference $\frac{1}{2}[R_{XY}(B+)-R_{XY}(B-)]$ has no Hall contribution, and closely follows the raw R_{XX} data at the same front-gate voltage. Such analysis for the low-filling fractional QH regime has been reported in Ref. 34.

The second technique is approximate; it is exact in certain bulk-edge network models of QH transport,[35–38] and is also an approximate semiclassical result in the limit of $\sigma_{XX}\ll\sigma_{XY}$ in 2D samples.[39] For each V_{FG} in Fig. 2, we subtract the longitudinal from the Hall magnetoresistance, $R_{XY}(B)-R_{XX}(B)$, both for $B+$. When both, constriction and the bulk, are on a QH plateau, it is apparent that the difference is h/f_Be^2, the bulk Hall effect. However, this technique also subtracts the finite σ_{XX} contributions in the transition regions between the plateaus, equally present in both R_{XY} and R_{XX} (as shown in Fig. 6).

The fine structure in the traces of Figs. 2–6 is attributed to disorder-assisted tunneling and quantum interference effects. It is particularly visible in the difference data of Fig. 6 for the more constricted sample (more negative V_{FG}). The individual R_{XY} and R_{XX} traces for the same V_{FG} were taken several days apart so that the detailed B-positions and magnitude of the "mesoscopic features" do not match, and thus do not subtract, due to their slow drift as a function of time. Aharonov-Bohm oscillations,[13–18] present in some data, have small amplitude ($\leq 4\times 10^{-3}$ h/e^2) and are not visible on the scale of Figs. 2–6.

B. Constriction electron density

The $B=0$, $V_{FG}=0$ shape of the electron density profile resulting from etch trench depletion in the interferometer region of the sample is illustrated in Fig. 1 of Ref. 24. The interferometer island is large, contains $2-4\times10^3$ electrons, and the 2D electron density profile is determined mostly by the classical electrostatics, minimizing the energy of electron-electron repulsion, compensated by attraction to the positively charged donors. The Fabry-Perot device depletion potential has saddle points in the constrictions, and so has the resulting electron density profile. In a quantizing magnetic field edge channels form, but the overall electron density profile closely follows the $B=0$ profile in these relatively large devices so as to minimize total Coulomb energy.

Because the in-plane screening by 2D electrons is relatively weak,[6,7,10] application of a negative front-gate voltage V_{FG} decreases electron density throughout the interferometer region. The main depletion is provided by the etch trenches; modeling[14,16,22] shows that application of a moderate V_{FG}, besides the overall depletion, increases effective depletion length by ~ 100 nm/V. Changing the magnetic field affects the equilibrium electron density profile in the device only weakly; particularly for $f \geq 4$, the principal effect is to redistribute the electron occupation between various Landau levels. In a fixed B, when the density of states in each Landau level in a given area is fixed also, application of V_{FG} changes occupation of these states.

We model the constriction following the Fock-Darwin model[40–42] for noninteracting electrons as a 1D conductor with a parabolic confining potential with energy level (1D subbands) spacing $\hbar\omega_0$. In a quantizing magnetic field with cyclotron energy $\hbar\omega_C$, hybrid magnetoelectric subbands with a bottom at energy $E_n=(n+\frac{1}{2})\sqrt{(\hbar\omega_0)^2+(\hbar\omega_C)^2}$, where $n=0,1,2,\ldots$, serve as conduction channels. In GaAs, spin splitting of the subbands is small compared with $\hbar\omega_C$, and develops only at higher magnetic fields. As $\hbar\omega_C \propto B$ is increased from zero, these magnetoelectric subbands cross the chemical potential, become depopulated, and so the number of the constriction conduction channels decreases. We use the experimental number of constriction conduction channels, taken as f_C from the corresponding constriction plateau position (the exact filling $\nu=f$) in the magnetoresistance data in Fig. 2 [shown as circles in Fig. 7(a)]. Both $R_{XX}(B)$ and $R_{XY}(B)$ data sets yield consistent constriction plateau positions; the horizontal error bars represent the uncertainty in the B-position of the centers of the plateaus.

Each set of channel number $\{f, B_f\}$ points, corresponding to a particular V_{FG}, is fitted with

$$f = f_0/\sqrt{1+(f_0 B_f/B_1)^2}, \tag{1}$$

where f_0 is the conduction channel number at $B=0$, and B_1 is the $f=1$ plateau center; both refer to constriction. The fits, shown in Fig. 7(a), were performed for the data for V_{FG} stepped typically by 60 mV; they yield f_0 as the best fit parameter, plotted in Fig. 7(b). One $f_0=582\pm300$ for $V_{FG}=+100$ mV is not shown in Fig. 7(b). The value of $f_0 \sim 100$ at zero front-gate bias is consistent with the four-terminal sample resistance of $\sim 300\ \Omega$ at 1.2 K. (At mK temperatures, the $B=0$ sample resistance is higher, ~ 1.2 kΩ, as can be seen in Fig. 2, likely due to quantum interference effects in the device.) The absolute error in f_0 is, unsurprisingly, large for nearly open constriction, when the constriction density is only slightly less than n_B.

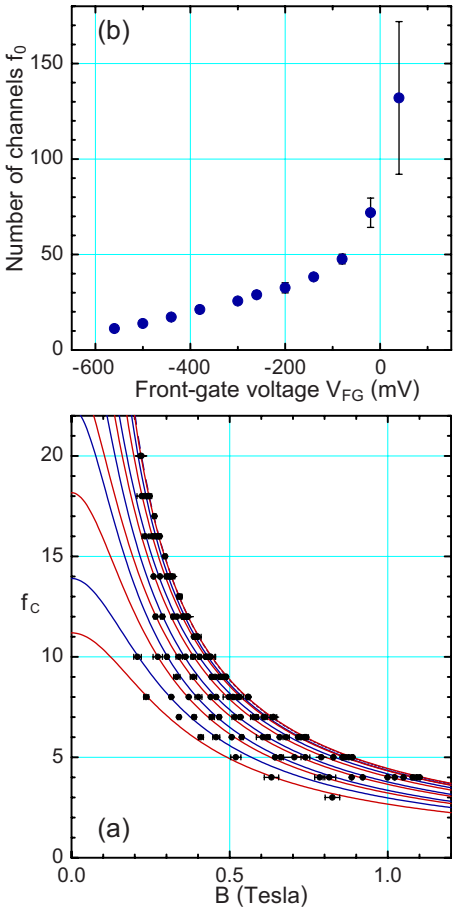

FIG. 7. (Color online) (a) Positions of the constriction plateaus from the data of Fig. 2 (circles with horizontal error bars) and the fits to the 1D Fock-Darwin model (lines). Each set of points and the fit correspond to a particular V_{FG}. (b) Zero-field number of conduction channels in the constriction obtained from the fits shown in (a).

The second fit parameter, B_1, gives information on constriction density, $n_C=eB_1/h$ at $\nu_C=1$. Thus obtained constriction density is plotted as a function of V_{FG} in Fig. 8. Since n_C is derived from the QH transport data, it should correspond to the electron density near the saddle point in the constriction, which determines the constriction QH filling. We also have determined the constriction density as $n_C=\nu eB/h$ from the raw transport data Hall slope (crosses in Fig. 8). The classical Hall line is forced through zero at $B=0$, which results in a systematically larger Hall slope, and so underestimates n_C. Roughly, this procedure is equivalent to the Fock-Darwin analysis described above, but setting $f_0 \to \infty$ in Eq. (1).

Within the Fock-Darwin model, that is, assuming parabolic confinement potential and neglecting electron interaction, we can also estimate the constriction width[43,44] at chemical potential as $W \approx \pi f_0/2k_F \approx f_0\sqrt{\pi/8n_C}$. The resulting width varies as $280\ \text{nm} \leq W \leq 11\,000$ nm in the experi-

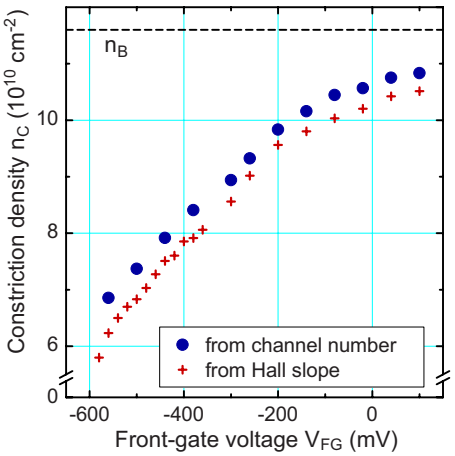

FIG. 8. (Color online) Constriction electron density obtained from the conduction channel number analysis, Eq. (1), in Fig. 7(a) (circles). Also shown is n_C obtained by conventional Hall slope (forced through zero) analysis (crosses). This neglects confinement in the constriction, and thus systematically underestimates the density. The 2D bulk density n_B is shown by the dashed line.

mental range of V_{FG}. The lower value of W is still larger than the tunneling distance of 100 nm, estimated from the amplitude of the Aharonov-Bohm oscillations.[20,21] The larger value, 11 μm, is much larger than the lithographic constriction width of 1.2 μm, and thus is not realistic. Both assumptions of the model are not realistic, and it is remarkable that some values obtained, such as f_0 and n_C, are reasonable, while others, such as W, are not.

Several words are in order regarding the island center electron density n_I. Etch trench depletion modeling at $V_{FG}=0$ gives $n_I \sim 2\%$ lower than n_B, and $\sim 7\%$ greater than constriction saddle-point density n_C.[24,45] This is consistent with the results shown in Fig. 8, giving $n_C \approx 0.92 n_B$ at $V_{FG}=0$. While present QH transport experiments do not probe n_I, an analysis of V_{FG} dependence of the period of the Aharonov-Bohm oscillations at lower filling $f \leq 4$ integer QH plateaus has led us to conclude that n_C decreases proportionately less than n_I, upon application of a negative V_{FG}.[16,22] This experimental conclusion is counterintuitive, but can be understood if one considers that the front gates have long leads and surround the island, while being only to one side of a constriction (Fig. 1). Accordingly, the island QH edge channels, which follow the constant electron density contours with density equal that in the constrictions, move inward, towards the island center, the interference path area shrinks, and the Aharonov-Bohm period increases.

IV. CONCLUSIONS

In conclusion, we have presented a comprehensive experimental characterization of quantum Hall and Shubnikov-de Haas transport in an electron Fabry-Perot interferometer. We find that application of front-gate voltage affects the constriction electron density, while the bulk density remains unaffected. This results in quantized plateaus in longitudinal resistance, while the Hall resistance is dominated by the low-density, low-filling constriction. At lower fields, when the quantum Hall plateaus fail to develop, we observe bulk Shubnikov-de Haas oscillations in series, corresponding to an integer filling of the magnetoelectric subbands in the constriction. We conclude that the whole interferometer region is still quantum coherent at these lower fields at 10 mK. From a Fock-Darwin analysis, we obtain the constriction electron density as a function of the front-gate bias and the zero-field number of 1D electric subbands (conductance channels) resulting from the electron confinement in the constrictions.

ACKNOWLEDGMENTS

We thank Wei Zhou for help in experiments. This work is supported in part by the National Science Foundation under Grant No. DMR-0555238.

*Present address: Center for Functional Nanomaterials, Brookhaven National Laboratory, Upton, NY 11973.

[1] K. von Klitzing, G. Dorda, and M. Pepper, Phys. Rev. Lett. **45**, 494 (1980).
[2] *The Quantum Hall Effect*, 2nd ed., edited by R. E. Prange and S. M. Girvin (Springer, New York, 1990).
[3] D. Yoshioka, *The Quantum Hall Effect* (Springer, New York, 2002).
[4] R. B. Laughlin, Rev. Mod. Phys. **71**, 863 (1999).
[5] X. G. Wen, Int. J. Mod. Phys. B **6**, 1711 (1992).
[6] D. B. Chklovskii, B. I. Shklovskii, and L. I. Glazman, Phys. Rev. B **46**, 4026 (1992).
[7] B. Y. Gelfand and B. I. Halperin, Phys. Rev. B **49**, 1862 (1994).
[8] S. Ihnatsenka and I. V. Zozoulenko, Phys. Rev. B **77**, 235304 (2008) and references therein.
[9] A. Baumgartner, T. Ihn, K. Ensslin, K. Maranowski, and A. C. Gossard, Phys. Rev. B **76**, 085316 (2007) and references therein.
[10] G. F. Giuliani and G. Vignale, *Quantum Theory of the Electron Liquid* (Cambridge University Press, Cambridge, 2005).
[11] B. J. van Wees *et al.*, Phys. Rev. Lett. **60**, 848 (1988).
[12] D. A. Wharam *et al.*, J. Phys. C **21**, L209 (1988).
[13] H. van Houten, C. W. J. Beenakker, and A. A. M. Staring, in *Single Charge Tunneling*, edited by H. Grabert and M. H. Devoret (Plenum, New York, 1992).
[14] F. E. Camino, W. Zhou, and V. J. Goldman, Phys. Rev. B **72**, 155313 (2005).
[15] W. Zhou, F. E. Camino, and V. J. Goldman, *Proceedings of the 24th International Conference on Low Temperature Physics*, AIP Conf. Proc. No. 850 (AIP, Melville, 2006), p.1351.
[16] F. E. Camino, W. Zhou, and V. J. Goldman, Phys. Rev. B **76**, 155305 (2007).
[17] L. P. Kouwenhoven *et al.*, Surf. Sci. **229**, 290 (1990).
[18] M. D. Godfrey, P. Jiang, W. Kang, S. H. Simon, L. N. Pfeiffer, K. W. Baldwin, and K. W. West, arXiv:0708.2448 (unpublished).

[19] C. M. Marcus (private communication).
[20] F. E. Camino, W. Zhou, and V. J. Goldman, Phys. Rev. Lett. **95**, 246802 (2005).
[21] F. E. Camino, W. Zhou, and V. J. Goldman, Phys. Rev. B **72**, 075342 (2005).
[22] W. Zhou, F. E. Camino, and V. J. Goldman, Phys. Rev. B **73**, 245322 (2006).
[23] F. E. Camino, W. Zhou, and V. J. Goldman, Phys. Rev. B **74**, 115301 (2006).
[24] F. E. Camino, W. Zhou, and V. J. Goldman, Phys. Rev. Lett. **98**, 076805 (2007).
[25] R. L. Willett, M. J. Manfra, L. N. Pfeiffer, and K. W. West, arXiv:0807.0221 (unpublished).
[26] V. J. Goldman and B. Su, Science **267**, 1010 (1995).
[27] C. Nayak, S. H. Simon, A. Stern, M. Freedman, and S. Das Sarma, Rev. Mod. Phys. **80**, 1083 (2008).
[28] P. Bonderson, A. Kitaev, and K. Shtengel, Phys. Rev. Lett. **96**, 016803 (2006).
[29] A. Stern, Ann. Phys. **323**, 204 (2008).
[30] P. Bonderson, M. Freedman, and C. Nayak, arXiv:0808.1933 (unpublished).
[31] M. Shayegan, V. J. Goldman, M. Santos, T. Sajoto, L. Engel, and D. C. Tsui, Appl. Phys. Lett. **53**, 2080 (1988).
[32] R. J. Haug, A. H. MacDonald, P. Streda, and K. von Klitzing, Phys. Rev. Lett. **61**, 2797 (1988).
[33] L. D. Landau and E. M. Lifshitz, *Electrodynamics of Continuous Media*, 2nd ed. (Pergamon, London, 1984), Vol. 8, Chap. 3.
[34] V. J. Goldman, J. K. Wang, B. Su, and M. Shayegan, Phys. Rev. Lett. **70**, 647 (1993).
[35] A. H. MacDonald and P. Streda, Phys. Rev. B **29**, 1616 (1984).
[36] M. Buttiker, Phys. Rev. B **38**, 9375 (1988).
[37] J. K. Jain and S. A. Kivelson, Phys. Rev. B **37**, 4276 (1988).
[38] J. K. Wang and V. J. Goldman, Phys. Rev. B **45**, 13479 (1992).
[39] I. M. Ruzin, S. Marianer, and B. I. Shklovskii, Phys. Rev. B **46**, 3999 (1992).
[40] V. Fock, Z. Phys. **47**, 446 (1928).
[41] C. G. Darwin, Proc. Cambridge Philos. Soc. **27**, 86 (1931).
[42] R. B. Dingle, Proc. R. Soc. London, Ser. A **211**, 500 (1952).
[43] S. B. Kaplan and A. C. Warren, Phys. Rev. B **34**, 1346 (1986).
[44] B. J. van Wees *et al.*, Phys. Rev. B **38**, 3625 (1988).
[45] A. Siddiki (private communication).